

## Line Shapes of High Resolution Photoassociation Spectra of Optically Cooled Atoms

Reginaldo Napolitano and John Weiner

*Department of Chemistry and Biochemistry, University of Maryland, College Park, Maryland 20742*

Carl J. Williams

*James Franck Institute, University of Chicago, 5640 Ellis Avenue, Chicago, Illinois 60637*

Paul S. Julienne

*Molecular Physics Division, National Institute of Standards and Technology, Gaithersburg, Maryland 20899*

(Received 16 March 1994)

High resolution photoassociation spectra of colliding ultracold trapped atoms contain detailed information about ground and excited state interactions. We calculate the asymmetric line shapes for ultracold Na<sub>2</sub> absorption using a resonance scattering expression, proportional to a free-bound Franck-Condon factor, that is justified by full quantum scattering calculations of a collision in a radiation field. The line shapes illustrate Wigner threshold law behavior, which is characteristic of the quantum limit as  $T \rightarrow 0$ . Using an adiabatic hyperfine analysis, we calculate and compare a model spectra for  $J = 1, 2, 3,$  and  $4$  features of the Na<sub>2</sub> <sup>1</sup>Π<sub>g</sub> ( $v = 48$ ) state to recent high resolution experimental data.

PACS numbers: 34.50.Rk, 32.80.Pj, 33.70.Ca

Photoassociation spectroscopy, first proposed by Thorsheim, Weiner, and Julienne [1] and recently observed by several groups [2–5], is a high resolution probe of molecular states formed by photoexciting two colliding cold atoms to an excited molecular dimer state. When the kinetic energy  $\varepsilon$  of two colliding ground state atoms plus photon energy  $\hbar\omega$  of a tunable laser matches the energy difference between an excited bound level  $b$  and the asymptotic ground state energy, photoexcitation will result in level  $b$ , appearing as a scattering resonance. If the bound level decays to some product state  $p$ , which is detected as a function of  $\hbar\omega$ , the resulting spectrum maps out the positions of the excited bound levels  $b$ . Because the thermal energy  $k_B T$  of trapped atoms is typically close to the natural linewidth of the atomic cooling transition, the high resolution photoassociation spectrum exhibits only slight thermal broadening.

Using a Breit-Wigner resonance scattering treatment and assuming that the natural width  $\gamma$  (in energy units) of the resonances was small compared to  $k_B T$ , Thorsheim, Weiner, and Julienne obtained a thermally averaged spectrum for Na atoms at 10 mK. Since  $T < 1$  mK in magneto-optical trap (MOT) [2–4] and far off-resonance trap (FORT) [5] experiments, we present a new treatment of the line shapes for photoassociation spectra valid even when  $k_B T < \gamma$ . Recently, 1 MHz resolution line shapes have been reported for both Na [2] and Rb [5] photoassociative spectra. These ultracold experiments confirm the prediction that detailed information on the ground state potential and scattering wave function can be obtained from line shapes and intensity patterns. Thus, experimental photoassociation spectra in conjunction with theoretical analysis should permit an accurate determination of scattering lengths and other ground state  $T \rightarrow 0$  collision properties relevant to achieving Bose-Einstein condensation in alkali systems [6].

Photoassociation spectrum is proportional to the rate coefficient  $K_p(T, \omega)$  for the inelastic process yielding product  $p$  from two colliding ground state <sup>2</sup>S atoms:

$$K_p(T, \omega) = \left\langle \frac{\pi v}{k^2} \sum_{l=0}^{\infty} (2l+1) |S_p(\varepsilon, l, \omega)|^2 \right\rangle, \quad (1)$$

where  $\varepsilon = \hbar k^2/2\mu$  is the asymptotic kinetic energy of the ground state <sup>2</sup>S + <sup>2</sup>S atoms,  $\mu$  is the reduced mass,  $l$  is the relative angular momentum quantum number, and  $S_p(\varepsilon, l, \omega)$  is the  $S$ -matrix element for the process that forms product  $p$  from the initial ground state channel. The brackets  $\langle \dots \rangle$  imply an average over the distribution of initial velocities  $v$ . If a Maxwellian distribution at temperature  $T$  is assumed, then

$$K_p(T, \omega) = \frac{k_B T}{h Q_T} \sum_{l=0}^{\infty} (2l+1) \int_0^{\infty} |S_p(\varepsilon, l, \omega)|^2 e^{-\varepsilon/k_B T} \frac{d\varepsilon}{k_B T}, \quad (2)$$

where  $Q_T = (2\pi\mu k_B T/h^2)^{3/2}$  is the translational partition function. Introducing  $k_B T$  twice in Eq. (2) expresses  $K_p$  in terms of the standard rate factor  $k_B T/h Q_T$  times a dimensionless quantity.

Our full quantum close coupling calculations show that the following simple resonant scattering expression for an isolated resonance  $b$  is an excellent approximation at MOT temperatures:

$$|S_p(\varepsilon, l, \Delta_b)|^2 = \frac{\gamma_p \gamma_s(\varepsilon, l)}{(\varepsilon - \Delta_b)^2 + (\gamma/2)^2}, \quad (3)$$

where  $\Delta_b(\omega) = E_b - \hbar\omega$  is the detuning relative to the position  $E_b$  of the bound state;  $\Delta_b$  is positive for  $\hbar\omega < E_b$  (red detuning) and negative for  $\hbar\omega > E_b$  (blue detuning); see Fig. 1. The total width (in energy units) of the excited

bound state is  $\gamma = \gamma_p + \gamma_s(\varepsilon, l) + \gamma_0$ , where  $\gamma_p/\hbar$  is the rate by which the bound state resonance  $b$  decays to the detected product  $p$ ,  $\gamma_s(\varepsilon, l)/\hbar$  is the stimulated emission rate back to the ground state, and  $\gamma_0/\hbar$  is the decay rate due to any other undetected processes (e.g., molecular predissociation). For low light intensity, Fermi's golden rule gives  $\gamma_s(\varepsilon, l) = 2\pi |\langle \varepsilon, l | V_{\text{rad}}(R) | b \rangle|^2$ , where the ground continuum wave function  $|\varepsilon, l\rangle$  is energy normalized, and  $V_{\text{rad}}(R) = (2\pi I/c)^{1/2} d(R)$  is the radiative coupling matrix element proportional to the square root of the probe laser intensity  $I$  and to the molecular transition dipole  $d(R)$ . We used two-state quantum close coupling calculations of a collision in a near resonant optical field to verify Eq. (3). These quantum calculations use an excited complex potential,  $V_e(R) - i\gamma_p(R)/2$ , coupled by  $V_{\text{rad}}(R)$  to the ground state potential  $V_g(R)$ ;  $V_g$  and  $V_e$  respectively approach 0 and  $\hbar(\omega_0 - \omega)$  in the atom-field state picture as  $R \rightarrow \infty$ , where  $\hbar\omega_0$  is the energy of the  $^2P_{3/2} + ^2S$  separated atoms. The term  $\gamma_p(R)/2$  describes the decay into the product channel, and  $|S_p(\varepsilon, l, \omega)|^2$  represents the loss of unitarity in the ground state channel due to decay of the excited resonance state to the product channel [7]. All calculations were carried out in the weak field limit, where  $\gamma_s(\varepsilon, l) \ll \gamma$ ,  $|S_p(\varepsilon, l, \omega)|^2 \ll 1$ , and the light shifts in  $\Delta_b$  can be neglected.

Evaluation of Eq. (3) requires a knowledge of the resonance positions  $E_b$ , the transition dipole moment  $d(R)$ , and the Franck-Condon factors. For  $V_g(R)$ , we either use the  $^3\Sigma_u$  hybrid Rydberg-Klein-Ress (RKR) *ab initio* potential of Ref. [1] (potential 1) or of Ref. [8] (potential 2). For  $V_e(R)$  we use the adiabatic  $1_g$  state found from diagonalizing the  $^2S + ^2P$  electronic + fine structure Hamiltonian for  $\text{Na}_2$  using the potentials from Magnier *et al.* [9]. The decay rate  $\gamma_p(R)$  is the spontaneous emission rate of the adiabatic  $1_g$  state, calculated as in Ref. [10] by diagonalizing this  $^2S + ^2P$  Hamiltonian, and

$d(R)$  is proportional to the square root of  $\gamma_p(R)$ . In our two-state model  $\gamma_s(\varepsilon, l)$  is calculated as if the ground state were degenerate, neglecting hyperfine structure. However, in order to properly calculate the relative intensities of the resonances in the experimental spectrum, full multichannel scattering wave functions which incorporate the ground state hyperfine structure must be used for  $|\varepsilon, l\rangle$  along with an additional sum over all degenerate incoming channels. Incorporating ground state hyperfine structure does not modify our essential conclusions, and we account for excited state hyperfine structure below. Both ground and excited state hyperfine structures can be incorporated together using the formalism described in Ref. [11].

The detailed thermal line shape,  $K_p(T, \Delta_b)$  vs  $\Delta_b$ , depends strongly on  $\gamma_s(\varepsilon, l)$  in the numerator and  $\gamma$  and  $\varepsilon - \Delta_b$  in the denominator of (3). The Wigner-law threshold effects enter  $K_p(T, \Delta_b)$  through the  $\varepsilon$  dependence of  $\gamma_s(\varepsilon, l)$ . This occurs at typical MOT temperatures, since  $\varepsilon$  is small compared to the energy  $\varepsilon_Q$  [12] characteristic of the onset of such effects:  $\varepsilon_Q$  is estimated to be 120, 20, 5, 1.5, and 0.6 mK, respectively for Li, Na, K, Rb, and Cs [13]. In the Wigner-law regime, i.e., at sufficiently small  $\varepsilon \ll \varepsilon_Q$ ,  $\gamma_s(\varepsilon, l) = A_l \varepsilon^{(2l+1)/2}$ . The magnitude of  $A_l$  and the deviation of  $\gamma_s(\varepsilon, l)$  from this simple functional dependence are extremely sensitive to fine details of the ground state potential. Figure 2 shows the variation of  $\gamma_s(\varepsilon, l)$  with  $\varepsilon/k_B$  for  $l = 0, 1$ , and  $2$  ( $s, p$ , and  $d$  waves) of the  $1_g$  ( $v = 48$ ) vibronic state and the ground  $^3\Sigma_u$  potentials of Refs. [1] and [8]. In calculating these results we have used  $\gamma_p/\hbar = 0.0746$  MHz,  $\gamma_0 = 0$ , and an  $R$ -independent  $V_{\text{rad}}/\hbar = 15.0$  MHz. The lines clearly exhibit the expected Wigner law variation and the two panels show the marked sensitivity to the potentials. Although only  $s$ -wave contributions to  $K_p(T, \Delta_b)$  remain nonvanishing in the  $T \rightarrow 0$  limit, experimental measurement [2], as well as these calculations, show that at the small but finite temperature in a Na MOT there are also significant contributions from ground  $p$  and  $d$  waves in addition to  $s$  waves.

Figure 3 shows calculated thermally averaged line shapes at  $T = 600 \mu\text{K}$  for absorption to the vibrational levels  $v = 48$  and  $v = 85$  of the  $1_g$  state for  $s, p$ , and  $d$  ground state collisions using potential 1. These line shapes are normalized to unity at the peak (relative  $s, p$ , and  $d$  peak intensities are 1.000, 0.583, and 0.442 for  $v = 48$  and 1.000, 0.665, and 0.077 for  $v = 85$ ). Although  $k_B T \ll \varepsilon_Q$ , it is possible for the relative intensity of the  $p$ - or  $d$ -wave feature to dominate the spectrum and this actually occurs when we use potential 2, where the relative  $s$ -,  $p$ -, and  $d$ -wave intensities for  $v = 48$  are 1.000, 8.644, and 0.026. There are two notable features of Fig. 3. First, the different Wigner law onset for  $s$ -,  $p$ -, and  $d$ -wave absorption shows up as an  $l$ -dependent shift in the position of the predicted absorption peak relative to the actual resonance position at  $\Delta_b = 0$ , with the actual shift being sensitive to the

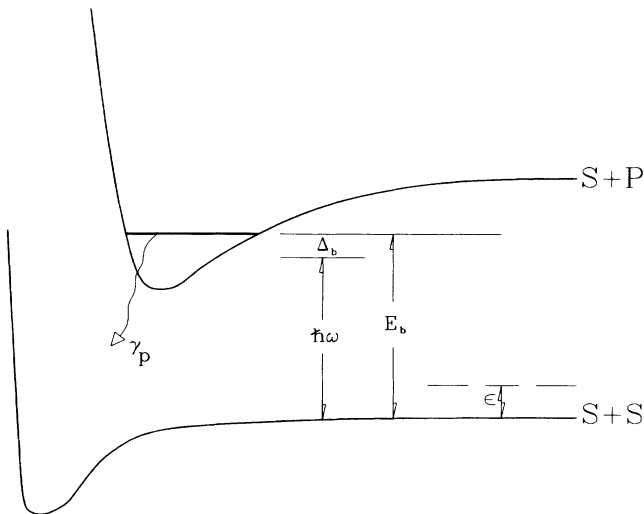


FIG. 1. Relevant energies, potential curves, and transitions for an isolated resonance in the photoassociation process.

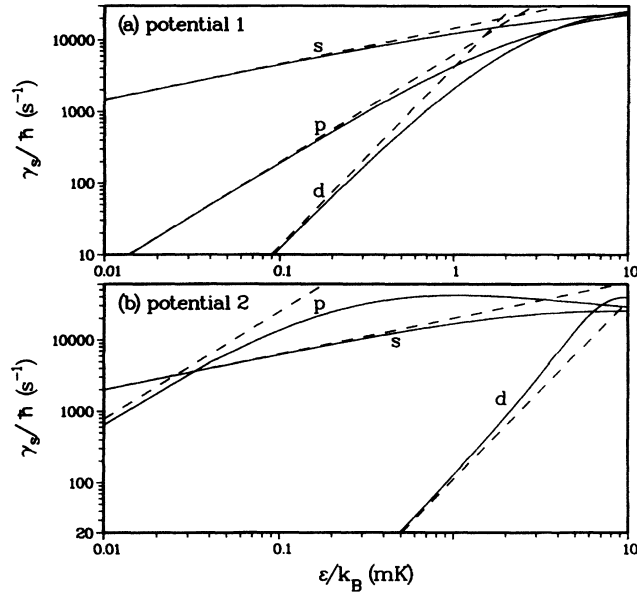


FIG. 2. Calculated  $\gamma_s(\epsilon, l)/\hbar$  vs  $\epsilon/k_B$  for  $l = 0, 1$ , and  $2$  for  $\nu = 48$ : (a) potential 1 of Ref. [1], (b) potential 2 of Ref. [8]. The dashed lines shows the Wigner law variation  $A_l \epsilon^{(2l+1)/2}$ . The primary difference between the two potentials is an adjustment of the dissociation energy by 5.1 GHz.

ground state potential. One consequence of this apparent shift is that experimental rotational constants, deduced from differences between measured positions of different total angular momentum states  $J$  [2,5], may contain small contributions from Wigner law shifts in peak position. Second, the  $\nu = 48$  and 85 features show significantly different shapes, especially in the onset of absorption in detuning from blue to red across the resonance. These shape differences are due to the very different lifetimes and radiative decay widths  $\gamma_p/\hbar$  of these levels. The transition dipole of the  $1_g$  state rapidly approaches zero as  $R$  decreases and the electronic binding energy becomes larger than the  ${}^2P(3/2)$ - ${}^2P(1/2)$  fine structure splitting. This is a result of the long range Hund's case (c)  $1_g$  state adiabatically transforming into a Hund's case (a)  ${}^1\Pi_g$  state at short range; decay of the Hund's case (a)  ${}^1\Pi_g$  state is dipole forbidden to either the  ${}^1\Sigma_g$  or  ${}^3\Sigma_u$  ground states. We calculate  $\gamma_p/\hbar = 0.0746$  and  $9.76$  MHz for the respective  $\nu = 48$  and 85 levels, corresponding to temperatures of  $\gamma_p/k_B = 3.58$  and  $468$   $\mu\text{K}$ . The narrow  $\nu = 48$  level exhibits almost no natural broadening on the scale of Fig. 3, where most of the broadening is purely thermal. In contrast, the large natural width of  $\nu = 85$  gives a resonance line shape comparable to the effect of thermal broadening resulting in a noticeably broader  $\nu = 85$  resonance.

In order to test whether  $T$  can be deduced from the red tail of the line shape, we have fit the line shapes in Fig. 3 to the exponential form  $\exp(-\Delta_b/k_B T)$ . Using the detuning range 20 to 70 MHz red of the peak position for  $\nu = 48$ , we deduce effective temperatures of 654, 718,

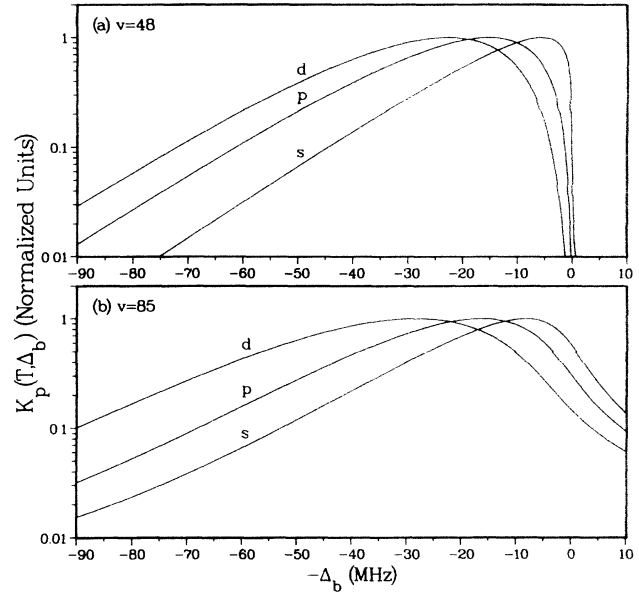


FIG. 3. Calculated  $K_p(T, \Delta_b)$ , normalized to unity at the peaks, vs  $-\Delta_b$  for (a)  $\nu = 48$  and (b)  $\nu = 85$ .

and  $753$   $\mu\text{K}$  from the *s*, *p*, and *d* line shapes. These temperatures are significantly larger than the reference  $T$  of  $600$   $\mu\text{K}$  in Fig. 3, because of the skewing of the shape by the Wigner law variation of  $\gamma_s(\epsilon, l)$  in the numerator. When we carry out the same fitting procedure for  $\nu = 85$ , the effective temperature deviates from  $600$   $\mu\text{K}$  by a much larger amount. We conclude that natural broadening and the proper Wigner onset must be taken into account to extract a temperature from measured line shapes.

Figure 4 compares our calculated spectra for the  $J = 1, 2, 3$ , and  $4$  features of the  $\text{Na}_2 1_g(\nu = 48)$  state with the NIST experimental high resolution spectra [2]. We use the line shapes of Fig. 3 for  $600$   $\mu\text{K}$  and calculate resonance positions taking into account the full hyperfine structure of the excited rotating molecule, according to the adiabatic approximation described in Ref. [14]. The relative intensities of different individual hyperfine resonances due to a given  $l$  wave in the ground state were obtained by spherically averaging the squared radiative coupling matrix elements  $V_{\text{rad}}(R)$  connecting the individual resonance to all channels of the two ground  $\text{Na}({}^2S, f = 1)$  hyperfine atoms. Since the relative magnitudes of the *s*-, *p*-, and *d*-wave Franck-Condon factors are sensitive to minor modifications in the ground state potential  $V_g(R)$ , we have varied the relative contributions of *s*, *p*, and *d* waves to qualitatively reproduce the  $J = 1$  feature. Although we produce the correct widths and number of peaks for the  $J = 2$  feature, including the small "shelf" and rapid *s*-wave onset behavior on the blue side, the peaks do not have the correct relative magnitudes. To obtain better agreement between theory and experiment for the line shapes and relative magnitudes of individual

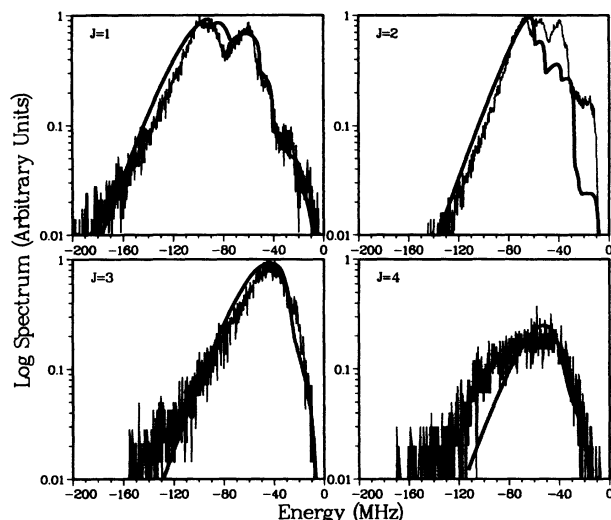


FIG. 4. Experimental high resolution spectra from the NIST laser cooling group for photoassociation to the  $\text{Na}_2 1_g v = 48$   $J = 1, 2, 3,$  and  $4$  levels (the  $J = 2$  data appear in Fig. 4 of Ref. [2(b)]), compared to theoretical simulations (thick solid line). The zero detuning position for each  $J$  is chosen as the bluest calculated hyperfine component with nonzero oscillator strength for the hyperfine cluster of lines for that  $J$ . The ground state partial waves contributing to the respective  $J = 1, 2, 3,$  and  $4$  clusters are  $s + p + d, s + p + d, p + d,$  and  $d$ ; contributions from  $l \geq 3$  are negligible for Na.

hyperfine components requires a full multichannel quantum treatment of the ground state scattering and improved ground state potentials. The  $J = 3$  and  $4$  line shapes show little hyperfine structure with the  $J = 4$  feature resulting entirely from ground state  $d$ -wave collisions. The calculated rise on the blue side for  $J = 4$  is much slower than the rapid  $s$ -wave onset for  $J = 2$ . Overall, the positions and widths of the hyperfine resonances are reproduced remarkably well.

We expect the study of intensity patterns in high resolution photoassociation spectra will prove to be a very powerful probe of ground state interactions and excited state dynamics. The number of spectral lines can be directly related to the number of partial waves that penetrate to small enough  $R$  to generate nonvanishing Franck-Condon factors. The major contribution to the Franck-Condon factor arises from the region around the outer turning point of the excited resonance level. Therefore, a plot of  $\gamma_s(\epsilon, l)$  versus  $E_b$  exhibits the characteristic Franck-Condon oscillations, predicted in Ref. [1] and observed in Refs. [2] and [5], reflecting the nodal structure of the ground state wave function in

the  $\epsilon \rightarrow 0$  limit. Because the relative intensities of the observed spectral features are very sensitive to details of the ground state potential, a precise analysis of high resolution photoassociation line shapes will determine the actual ground state potentials. Such potentials could then be used with confidence to predict collision rates and scattering length parameters required for modeling the approach to Bose-Einstein condensation in alkali atom traps [6].

We would like to thank the NIST experimental group (see Ref. [2]) for helpful discussions and especially for providing us with their high resolution data. R.N. acknowledges support by CNPq Brazil; J.W. acknowledges support by NSF and the Donors of the Petroleum Research Fund, administered by the American Chemical Society; C.J.W. acknowledges support of NSF, ONR, and NIST.

- [1] H. R. Thorsheim, J. Weiner, and P. S. Julienne, *Phys. Rev. Lett.* **58**, 2420 (1987).
- [2] (a) P. D. Lett, K. Helmerson, W. D. Phillips, L. P. Ratliff, S. L. Rolston, and M. E. Wagshul, *Phys. Rev. Lett.* **71**, 2200 (1993); (b) L. P. Ratliff, M. E. Wagshul, P. D. Lett, S. L. Rolston, and W. D. Phillips, *J. Chem. Phys.* **101**, 2638 (1994).
- [3] E. R. I. Abraham, N. W. M. Ritchie, W. I. McAlexander, and R. G. Hulet (unpublished).
- [4] V. Bagnato, L. Marcassa, C. Tsao, Y. Wang, and J. Weiner, *Phys. Rev. Lett.* **70**, 3225 (1993).
- [5] J. D. Miller, R. A. Cline, and D. J. Heinzen, *Phys. Rev. Lett.* **71**, 2204 (1993); R. A. Cline, J. D. Miller, and D. J. Heinzen *ibid.* **73**, 632 (1994).
- [6] E. Tiesinga, A. J. Moerdijk, B. J. Verhaar, and H. T. C. Stoof, *Phys. Rev. A* **46**, R1167 (1992); E. Tiesinga, B. J. Verhaar, and H. T. C. Stoof, *Phys. Rev. A* **47**, 4114 (1993).
- [7] P. S. Julienne, K.-A. Suominen, and Y. Band, *Phys. Rev. A* **49**, 3890 (1994).
- [8] W. T. Zemke and W. C. Stwalley, *J. Chem. Phys.* **100**, 2661 (1994).
- [9] S. Magnier, Ph. Millié, O. Dulieu, and F. Masnou-Seeuws, *J. Chem. Phys.* **98**, 7113 (1993).
- [10] M. Movre and G. Pichler, *J. Phys. B* **10**, 2631 (1977).
- [11] C. J. Williams, F. H. Mies, and P. S. Julienne (unpublished).
- [12] P. S. Julienne and F. H. Mies, *J. Opt. Soc. Am. B* **6**, 2257 (1989).
- [13] P. S. Julienne, A. M. Smith, and K. Burnett, *Adv. At. Mol. Opt. Phys.* **30**, 141 (1993).
- [14] C. J. Williams and P. S. Julienne, *J. Chem. Phys.* **101**, 2634 (1994).